SPECIAL PROJECT PROGRESS REPORT

All the following mandatory information needs to be provided. The length should *reflect the complexity and duration* of the project.

Reporting year	07/2026
Project Title:	Climate impacts of space-based geoengineering: EC-Earth simulations for optimal non-uniform radiative forcing by a Planetary Sunshade System
Computer Project Account:	spitmato
Principal Investigator(s):	Catello Leonardo Matonti
Affiliation:	Politecnico di Torino
Name of ECMWF scientist(s) collaborating to the project (if applicable)	Jost von Hardenberg, Shuting Yang
Start date of the project:	01 Jan, 2025
Expected end date:	31 December, 2026

Computer resources allocated/used for the current year and the previous one

(if applicable)
Please answer for all project resources

		Previous year		Current year	
		Allocated	Used	Allocated	Used
High Performance Computing Facility	(units)	19,000,000	10,592,432	19,000,000	10.707.869
Data storage capacity	(Gbytes)	40,000	10,000	40,000	10,000

Summary of project objectives (10 lines max)

The GeoMIP experiments G1, G1ext, G2 and G6Solar considered instantaneous or gradual variations of the solar constant and therefore did not address non-uniform radiative forcing through differential shading. This project uses a global climate model to address three core questions concerning a Planetary Sunshade System as a space-based strategy for solar radiation management: (a) What is the climate impact on Earth of different insolation patterns? (b) What are the effects during the transition phase before full deployment of the planetary sunshade? (c) Are the climatic effects of this mitigation strategy reversible?

Summary of problems encountered (10 lines max)

After verification of the IFS forcing interface, the main production issue arose in the coupled AOGCM integrations. At a small set of NEMO ocean-model grid points already affected by the local treatment in the domain-mask configuration (dommsk), numerical singularities and extreme velocities occasionally stopped the runs. Diagnosing these locations, testing the relevant masking and numerical-stability settings, and managing controlled restarts slowed production. The issue was traced to the ocean configuration rather than to the new solar-attenuation interface. Targeted stabilisation and careful restart management allowed the simulations to be completed. Additional effort was required to consolidate Climate Model Output Rewriter (CMOR)/NetCDF post-processing and paired diagnostics.

Summary of plans for the continuation of the project (10 lines max)

The next phase will extend the present work to a transient SSP2-4.5 scenario. Paired control and Planetary Sunshade System integrations will use evolving greenhouse-gas and aerosol forcing, with priority given to the fully coupled AOGCM response. The sunshade simulation will include gradual deployment, a period of full operation, and progressive dismantling, allowing both the effectiveness of the intervention and the reversibility of its climatic effects after termination to be assessed. The first experiment will use a global-coverage configuration. Subject to the available computational allocation, additional sensitivity experiments will be executed. The NEMO grid points previously affected by local numerical singularities will be monitored. The modified IFS code, technical documentation, and CMORised model outputs will be consolidated to ensure reproducibility and support future experiments.

List of publications/reports from the project with complete references

None so far.

Summary of results

If submitted **during the first project year**, please summarise the results achieved during the period from the project start to June of the current year. A few paragraphs might be sufficient. If submitted **during the second project year**, this summary should be more detailed and cover the period from the project start. The length, at most 8 pages, should reflect the complexity of the project. Alternatively, it could be replaced by a short summary plus an existing scientific report on the project attached to this document. If submitted **during the third project year**, please summarise the results achieved during the period from July of the previous year to June of the current year. A few paragraphs might be sufficient.

1. Scientific context and physical Planetary Sunshade concept

The project addresses limitations in both conventional solar-geoengineering experiments and current climate simulations of planetary sunshades. First, GeoMIP protocols such as G1, G1ext, G2 and G6Solar represent solar dimming by applying a prescribed scalar factor to the solar constant. A physical space-based occulting system, however, does not produce an exactly uniform perturbation, because the apparent overlap between a Planetary Sunshade System and the solar disc varies with the observer's latitude and longitude, local solar time, and season. Second, existing planetary-sunshade climate simulations do not simultaneously account for the bi-elliptic dynamics of the Sun–Earth–Moon system and use a fully coupled general circulation model in which both the atmosphere and ocean contribute to the climate response.

The first phase began with a bibliographic review of space-based solar geoengineering and an analytical description of the difference between natural daily-mean insolation and the insolation received in the presence of a disk-like sunshade near the Sun-Earth L1 region, composed by a swarm of solar sail satellites either assembled or orbiting around L1. The objective was to derive a horizontal attenuation factor that could be evaluated on the atmospheric grid and passed to the EC-Earth3 radiation scheme. Numerical tests confirmed that the simplifications introduced to avoid repeated evaluation of elliptic integrals produced negligible error for the initial uniform-disc case.

Generally, the Planetary Sunshade operates between the Sun and Earth, close to a photogravitational equilibrium displaced sunward of the classical Sun-Earth L1 point by solar-radiation pressure. Because both the Sun and the occulting system have finite apparent angular radii, three regimes are possible. In the umbra, the Sun is totally covered; in the penumbra, the discs overlap only partly; in the antumbra, the smaller apparent sunshade disc lies inside the solar disc and produces an annular occultation. The reference operating condition places Earth in the antumbra, producing partial and continuous attenuation rather than a total eclipse.

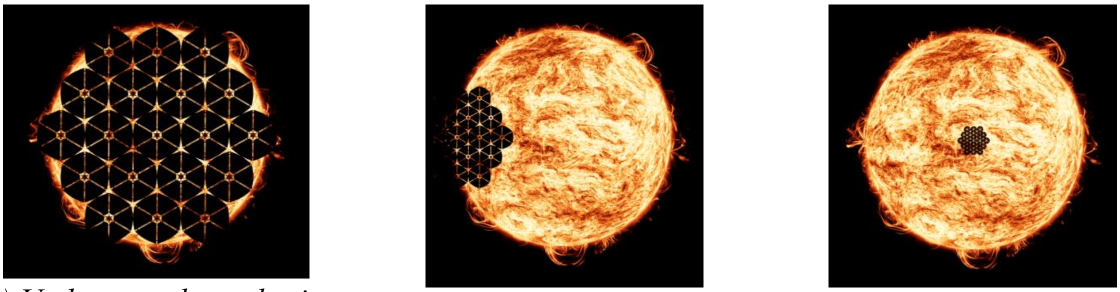

(a) Umbra: total occultation *(b) Penumbra: partial occultation* *(c) Antumbra: annular occultation*

Figure. Solar disc as observed from the umbra, penumbra and antumbra. The operational Planetary Sunshade attenuation is obtained from the visible fraction of the finite solar disc, not from a prescribed uniform reduction of the solar constant.

Because the apparent overlap varies among terrestrial locations at the same epoch, a single global attenuation percentage is adequate for first-order system sizing.

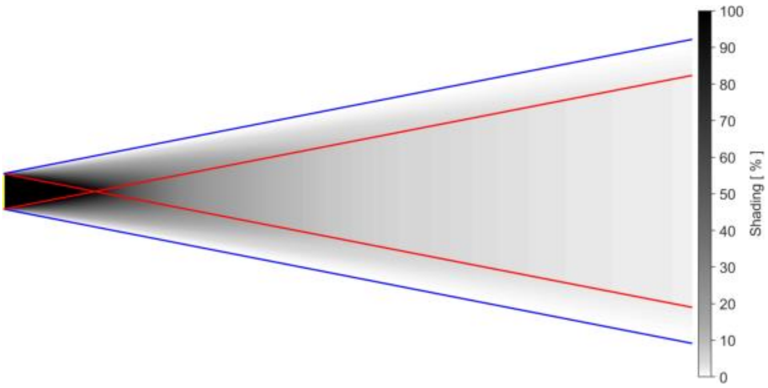

Figure. Planar section of the umbra, penumbra and antumbra generated by the finite Sun and Planetary sunshade disc; colour indicates the continuously varying shading intensity.

Indeed, at first order, the nominal circular-disc configuration reduces the incoming solar flux by 1.7%. A zero-dimensional energy-balance estimate gives a global-mean absorbed short-wave perturbation of approximately -4.0 W m^{-2} and an equilibrium temperature change of approximately -1.8 °C.

Then, the orbital model of the disc is formulated as a photogravitational bi-elliptic restricted four-body problem. The three massive bodies are the Sun, Earth and Moon, while each Solar-Sail Satellite is treated as a controlled massless body. Two prescribed Keplerian ellipses represent the dominant astronomical time dependence: the approximately annual outer motion of the Sun and the Earth-Moon centre of mass, and the approximately monthly inner motion of Earth and Moon around that centre of mass. At the photogravitational equilibrium, the solar radiation pressure shifts the operating point sunward of the classical L1 location. The minimum-mass solution for the reference 1.7% attenuation gives the following system-level quantities.

Quantity	Symbol	Reference value
Fractional solar-flux reduction	δQ/Q	0.017
Distance from Earth–Moon centre of mass	D	2.3665×10^6 km
Equivalent occulting radius	R	1.4362×10^3 km
Solar-sail lightness number	β	0.034942
Total equivalent sunshade mass	M	2.8393×10^{11} kg

The prescribed transverse motion and solar radiation pressure control law make the sunshade follows the actual Sun-Earth conjunction rather than the Sun-Earth/Moon-centre-of-mass line, in order to have the Earth and its centre of mass almost always aligned with the shadow cones main axis.

2. From orbital states to non-uniform forcing

At each grid point and radiation time step, the orbital solution provides the Planetary Sunshade position and projected occulting area. The optical model combines the Earth-Sun distance, solar-zenith angle, observer distances, and the apparent angular radii of the Sun and PSS to calculate C(φ, λ, t), the fraction of the solar disc that remains visible at latitude φ, longitude λ and time t. C = 1 denotes natural illumination, while smaller values denote partial occultation. The resulting field is passed to IFS, replacing a globally scaled solar constant with a physically generated grid-point forcing.

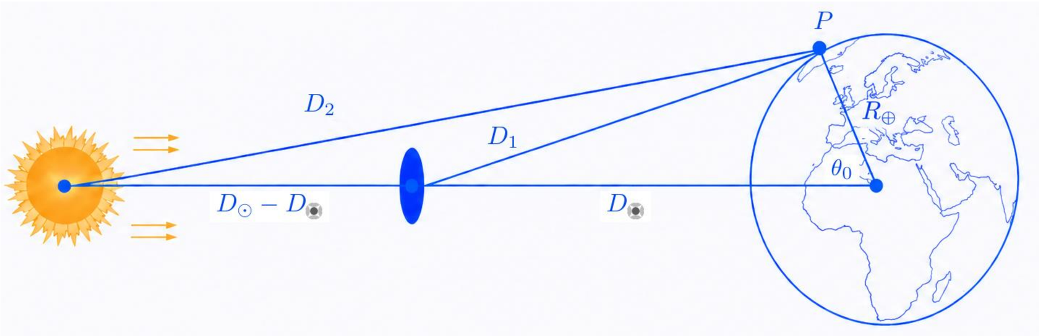

Figure. Centre-to-centre and observer-dependent distances used to transform the orbital state into apparent angular radii of the Sun and Planetary Sunshade for a terrestrial observer P.

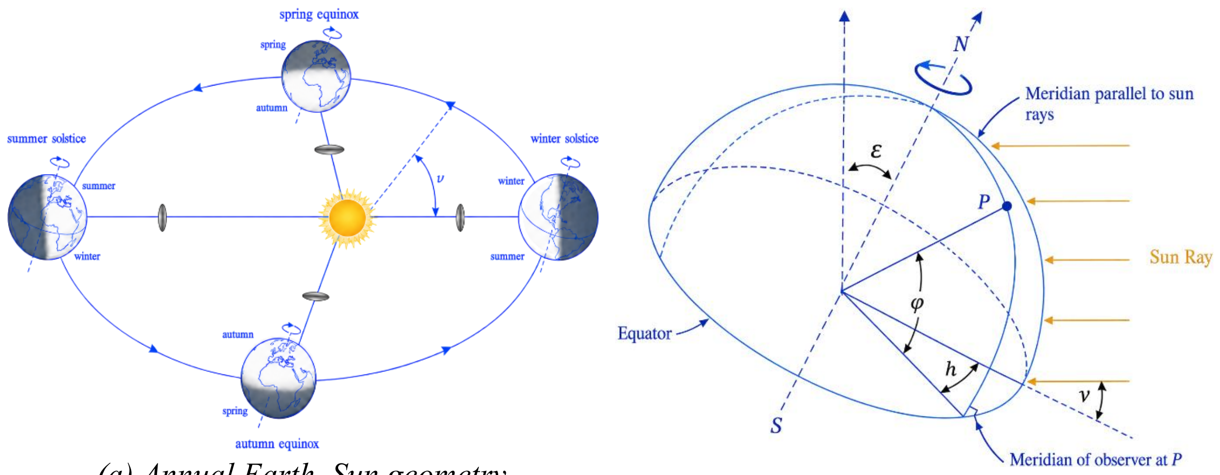

(a) Annual Earth–Sun geometry   *(b) Local solar geometry*

Figure. Solar geometry used to compute natural and Planetary Sunshade-modified insolation: annual orbital and seasonal evolution (left), and the local zenith-angle construction at latitude φ and local hour angle h (right).

The initial fixed-disc formulation already showed that a constant fractional occultation does not produce a spatially constant perturbation in W m⁻². Because natural solar flux varies with latitude, season and polar night, the absolute short-wave perturbation is largest in illuminated low latitudes and migrates during the year.

Implementing this field in EC-Earth3 required propagation of a horizontal attenuation array through the IFS radiation code. Early test integrations showed no difference between the control and sunshade cases because units and arguments were not propagated consistently across all subroutines. Systematic tracing and debugging resolved these issues, after which the expected reduction in incoming solar flux became visible. Compilation on the ECMWF ATOS system, restart handling and preliminary CMOR-compliant post-processing were also established during this phase.

Moreover, at each grid point, the cosine of the solar-zenith angle identifies the illuminated side of Earth. Night-side points receive zero direct solar flux. On the day side, the natural direct-normal irradiance is corrected for the instantaneous Earth-Sun distance and multiplied by C. Averaging over the illuminated part of one terrestrial rotation gives the daily-mean latitude-season field. The calculation retains Earth's obliquity, true anomaly and solar declination.

The resulting field retains the latitude-season pattern first verified analytically. Peak reductions approach -9.5 W m⁻² in illuminated low and middle latitudes, while polar-night regions remain near zero.

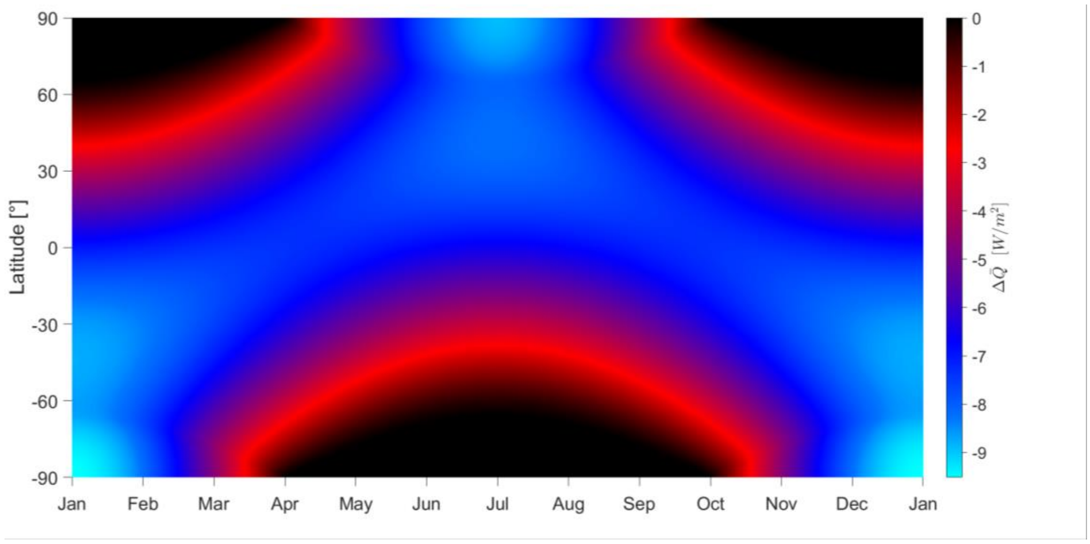

Figure. Analytical daily-mean change in top-of-atmosphere insolation between the initial sunshade case and natural illumination as a function of latitude and season.

3. EC-Earth3 implementation

The climate configuration couples the IFS cycle 36r4 for atmosphere and radiation, H-TESSEL for the land surface, NEMO 3.6 for the ocean, LIM3 for sea ice, and OASIS3-MCT for component exchange. The atmosphere uses TL255 spectral resolution, approximately 80 km horizontally, with 91 vertical levels. The ocean has a nominal 100 km grid, refined to approximately 40 km in the tropics, with 75 vertical levels. The attenuation factor is applied consistently when IFS reconstructs total-sky and clear-sky short-wave fluxes in the RADDIAG, RECMWF and RFMR radiation paths.

The experiment matrix comprises two Atmospheric Model Intercomparison Project (AMIP) configurations with prescribed sea-surface temperature and sea ice, and two Atmosphere-Ocean General Circulation Model (AOGCM) configurations with interactive NEMO ocean and LIM3 sea ice.

Simulation	Ocean/sea ice	Solar forcing	Purpose
AMIP control	Prescribed	Natural	Atmospheric reference
AMIP sunshade	Prescribed	Non-uniform sunshade	Fast atmosphere/land response
AOGCM control	Interactive NEMO/LIM3	Natural	Coupled reference
AOGCM sunshade	Interactive NEMO/LIM3	Non-uniform sunshade	Coupled climate response

Each simulation covers 30 model years with fixed 1990 external radiative forcing; monthly output extends through 2019. Every reported response is the Planetary Sunshade simulation minus its matching control. The additional AOGCM-minus-AMIP contrast identifies the response associated with interactive ocean and sea ice, but it is not interpreted as a pure ocean-feedback term because the lower boundary conditions and internal variability also differ. One realisation was completed for each configuration.

In EC-Earth/CMIP notation, rsdt is the incoming short-wave solar radiation at the top of the atmosphere (TOA), expressed in W m^{-2} and defined as positive downward. The corresponding upward fluxes are rsut, the reflected short-wave radiation, and rlut, the outgoing long-wave radiation. The net downward TOA energy flux is therefore N_{TOA} = rsdt - rsut - rlut. The sunshade produces a global-mean Δrsdt of approximately -5.8 W m^{-2} in both AMIP and AOGCM.

The temperature response differs strongly between the two configurations. With prescribed sea-surface temperature and sea ice, the AMIP global-mean near-surface air-temperature response remains near -0.1 K because only the atmosphere and land can adjust. In AOGCM, cooling starts at about -0.5 K, strengthens over several years, reaches approximately -1.6 to -1.9 K after the mid-2000s, and remains at that level through 2019. This contrast demonstrates the role of interactive ocean and sea ice.

The relevant comparison is between the paired anomalies because AMIP and AOGCM use different ocean boundary conditions. Since Δrsdt is nearly identical in both configurations, the small AMIP response does not indicate weak Planetary Sunshade forcing. Instead, prescribed sea-surface temperature prevents the ocean from storing and redistributing the energy deficit. In AOGCM, the coupled system integrates that deficit, progressively cooling the ocean-atmosphere state and modifying sea ice. The annual response becomes relatively stable after the mid-2000s, but the TOA diagnostics show that the system has not reached equilibrium.

The global mean hides the spatial structure. The AMIP anomaly is weak over prescribed-ocean regions and more evident over land, whereas the coupled experiment develops broad cooling with enhanced high-latitude responses. Local cooling exceeds 3 K in parts of the northern high latitudes. Because each configuration has a single realisation, regional anomalies should be interpreted qualitatively; the main result is the large-scale contrast between prescribed and interactive oceans.

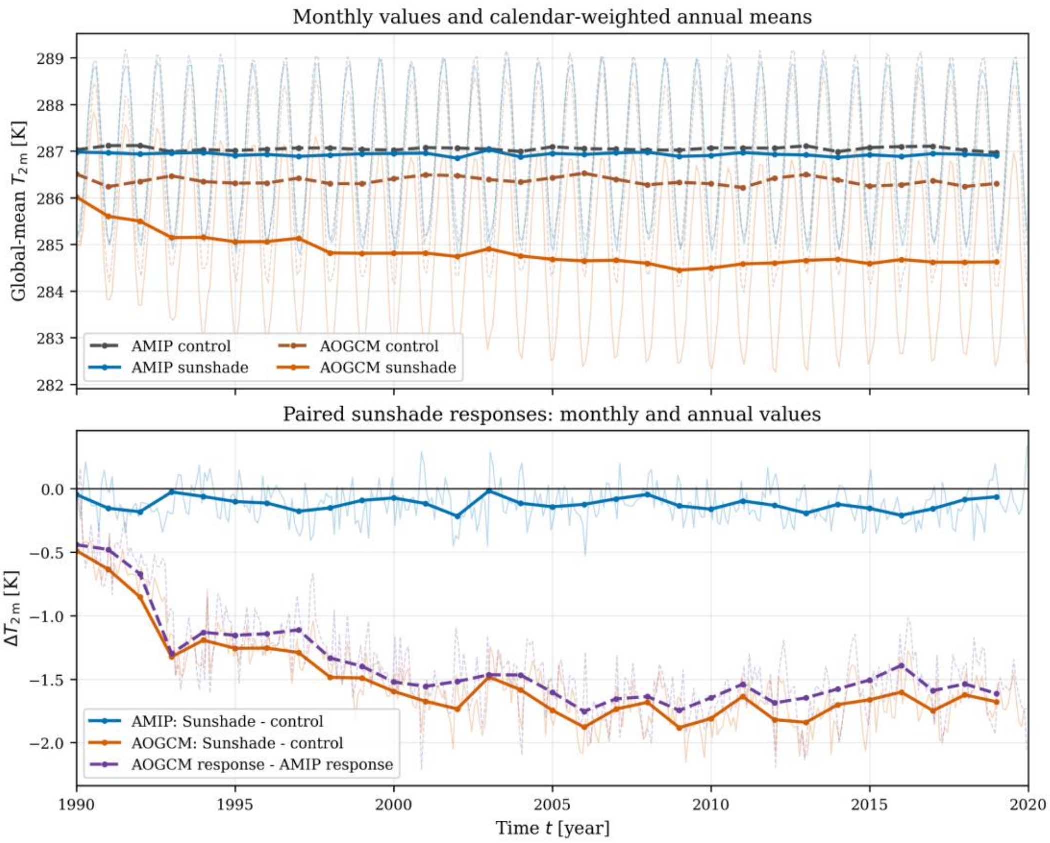

Figure. Global-mean near-surface air temperature in the four simulations and paired Planetary Sunshade responses. Thin curves are monthly values; thick curves are calendar-weighted annual means.

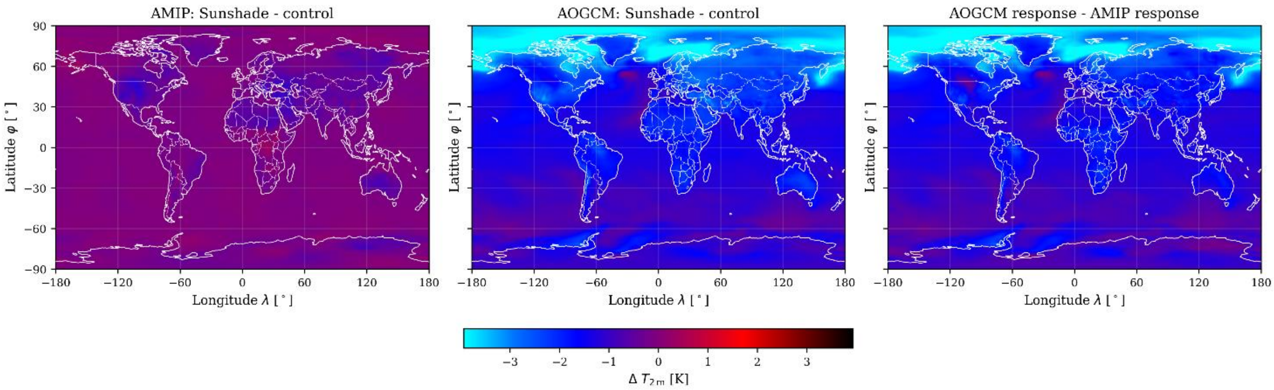

Figure. Climatological near-surface air-temperature response (Planetary Sunshade minus control) in AMIP and AOGCM, together with the coupled-minus-AMIP contrast, over the 30-year 1990–2020 plotting interval.

The temperature anomaly is not a direct geographical image of the imposed shadow. Atmospheric transport, ocean heat uptake and sea-ice feedback redistribute the initial short-wave perturbation. Enhanced coupled cooling at high latitudes is consistent with changes in sea ice, surface albedo and ocean heat transport, while the persistent low- and mid-latitude signal shows that the response is not confined to the latitudes of maximum instantaneous attenuation. The Hovmöller diagrams also show the coupled signal emerging progressively from monthly variability.

The fixed reduction in incoming sunlight produces different energy-budget adjustments. In AMIP, changes in reflected short-wave and outgoing long-wave radiation compensate only part of Δrsdt, leaving ΔN_TOA close to -3.5 W m^{-2}. This persistent deficit is expected because the prescribed ocean cannot cool. In AOGCM, the reduction in outgoing long-wave radiation increases as the climate cools, and ΔN_TOA evolves from about -3 W m⁻² toward approximately -1 W m⁻². The remaining negative value at year 30 shows that the coupled simulation has not fully equilibrated.

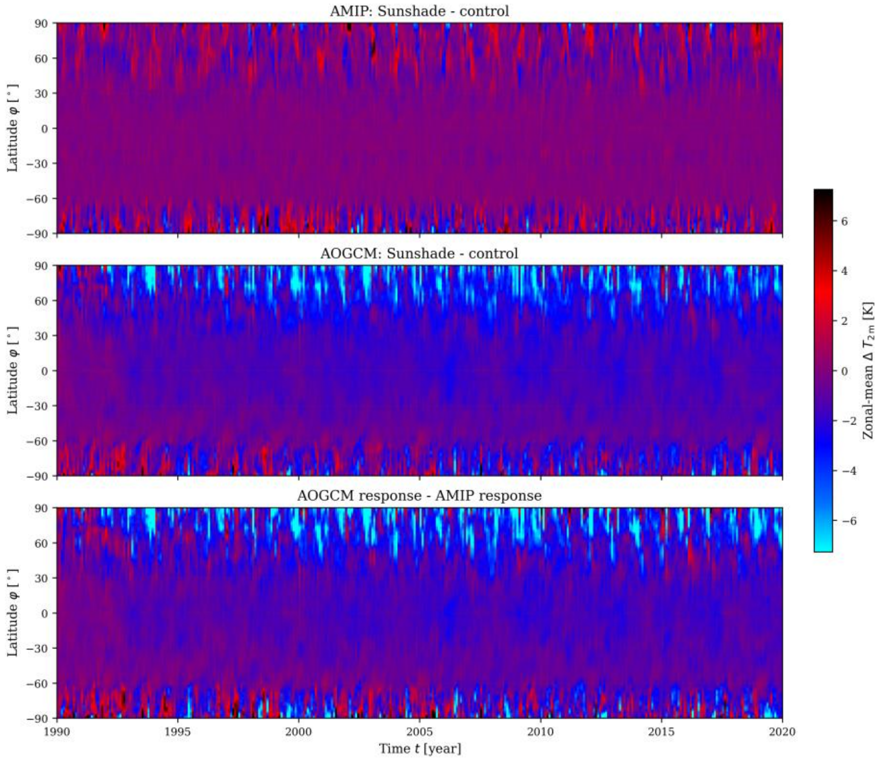

Figure. Zonal-mean monthly near-surface temperature response as a function of latitude and time for AMIP, AOGCM, and their difference. The coupled response develops progressively while the imposed optical perturbation remains fixed

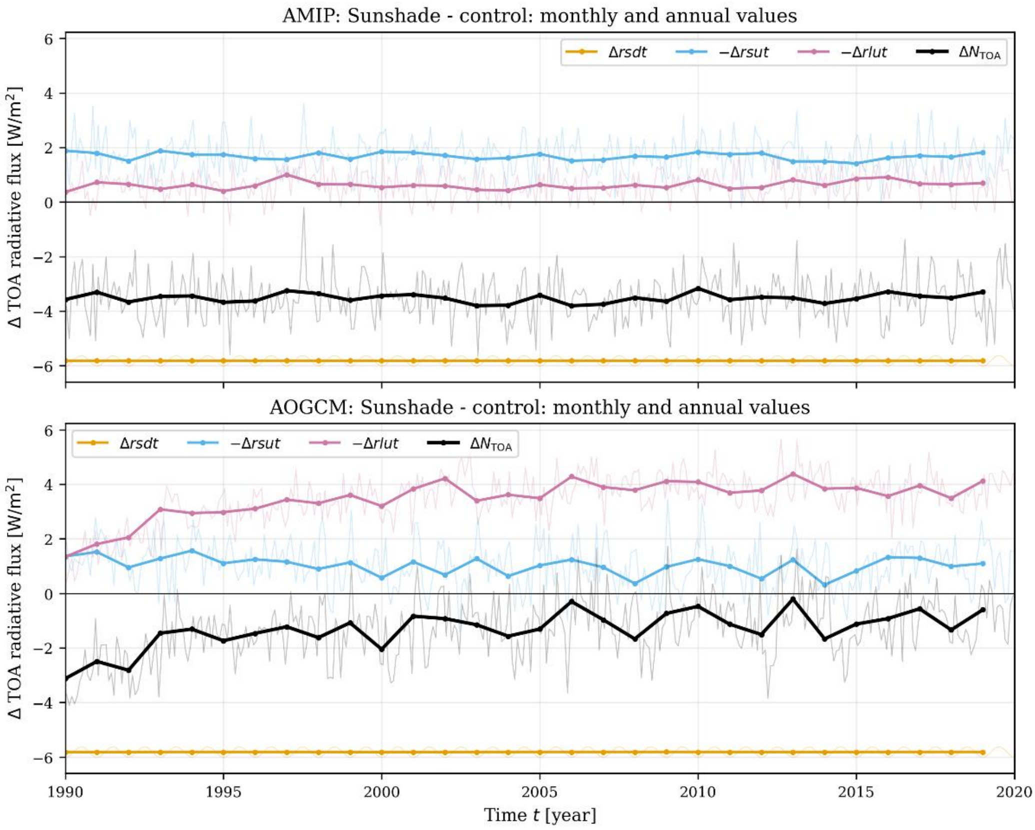

Figure. Contributions to the global-mean Planetary Sunshade-induced TOA energy-budget change. The plotted convention is positive toward the climate system, with ΔN_TOA = Δrsdt − Δrsut − Δrlut. Thin and thick curves show monthly and annual values.

The stronger AOGCM cooling therefore reflects the transient adjustment of an interactive ocean-sea-ice system to a sustained energy deficit, rather than a difference in the prescribed Planetary Sunshade attenuation.

The energy closure confirms this interpretation. Δrsdt remains almost constant near -5.8 W m^{-2}, as expected for a fixed optical forcing. As the coupled climate cools, outgoing long-wave radiation decreases, so -Δrlut becomes increasingly positive and offsets a growing fraction of the imposed deficit. ΔN_TOA consequently moves toward zero. Its residual value of roughly -1 W m^{-2} indicates that the system is still losing energy at the end of the integration; a final equilibrium response therefore cannot be inferred from these 30 years.

The variable rsds is downward short-wave radiation at the surface. It differs from rsdt because atmospheric absorption, scattering, clouds and surface reflection act between the TOA and the ground. The global AMIP response remains near -3 W m^{-2}, while the coupled response evolves from approximately -2.5 W m^{-2} toward values between 0 and -1 W m^{-2}.

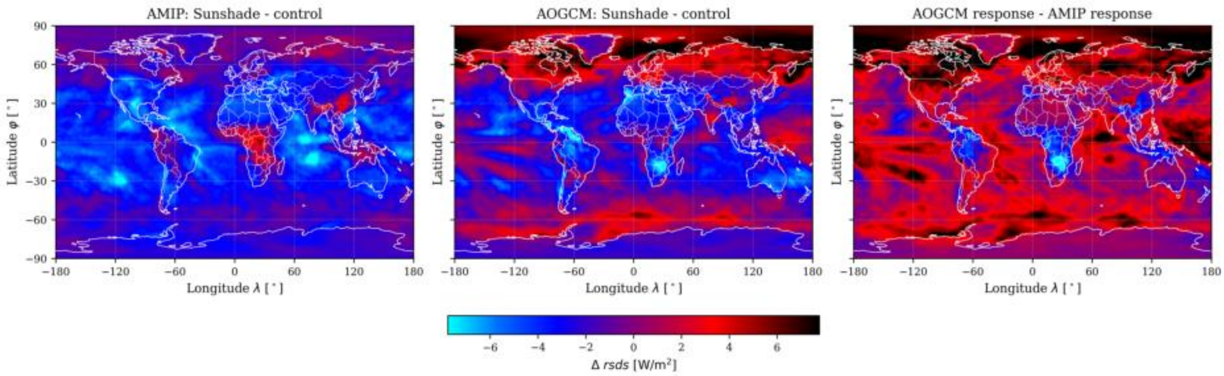

Figure. Climatological response of surface downwelling short-wave radiation (Δrsds) in AMIP, AOGCM and the coupled-minus-AMIP contrast over the 30-year interval.

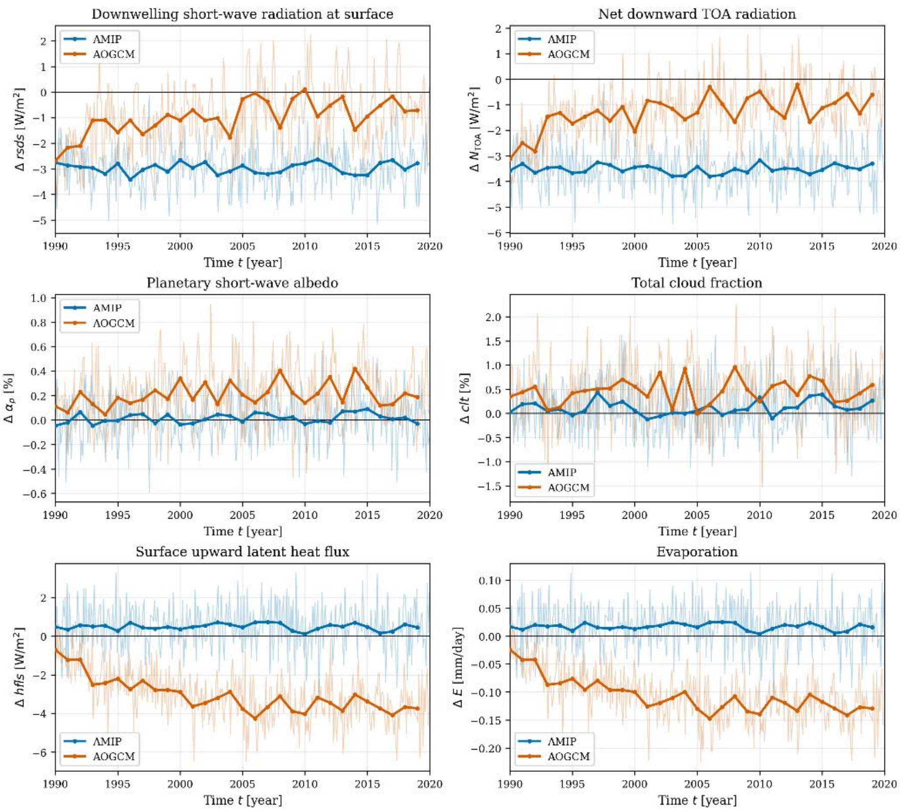

Figure. Global-mean paired responses of surface short-wave radiation, net TOA radiation, planetary albedo, total cloud fraction, upward latent-heat flux and evaporation.

Planetary albedo increases by roughly 0.1-0.4 percentage points and total cloud fraction by several tenths of a percentage point. The upward latent-heat-flux anomaly is about -4 to -3 W m^{-2}, and evaporation decreases by approximately 0.10-0.14 mm day^{-1}. These diagnostics indicate a weaker hydrological cycle under PSS forcing.

Locally positive surface short-wave anomalies do not indicate that the planetary sunshade adds solar energy since Δrsdt remains negative, while changes in cloud, atmospheric transmission and surface albedo can allow a larger fraction of the reduced TOA flux to reach the ground. Total cloud fraction alone cannot determine the sign of the cloud radiative feedback; that attribution requires cloud-radiative-effect and optical-property diagnostics.

Finally, large-scale circulation changes are smaller than the thermodynamic response but remain spatially structured. Sea-level-pressure anomalies reach local magnitudes of about 1.5 hPa, while near-surface wind-speed anomalies are mostly within 0.3 m s^{-1}.

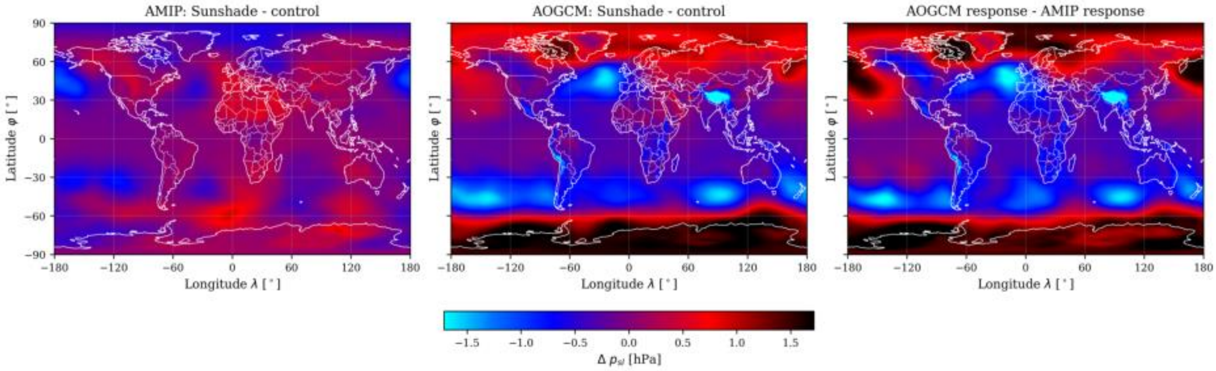

Figure. Climatological sea-level-pressure response in AMIP, AOGCM and their difference over the 30-year interval.

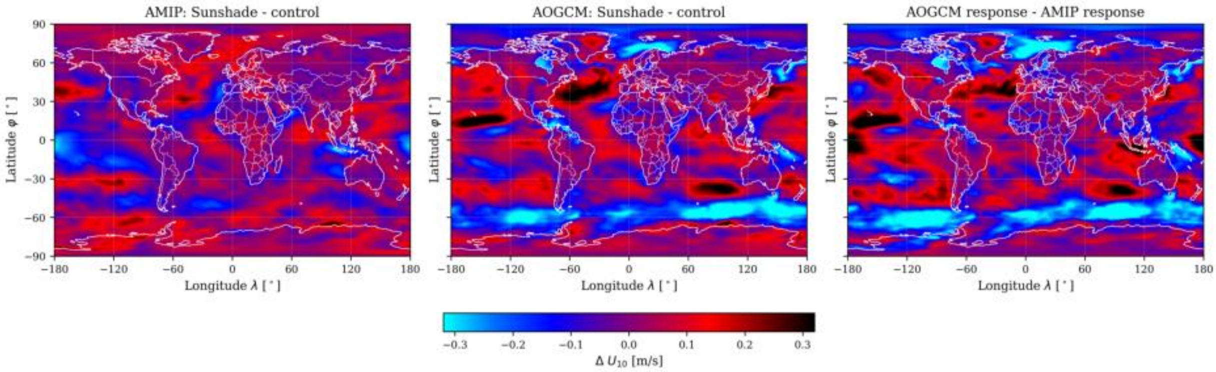

Figure. Climatological near-surface wind-speed response in AMIP, AOGCM and their difference over the 30-year interval.

The circulation response is modest in global magnitude but organised into regional bands and centres of action. The coupled solution shows more pronounced regional anomalies than AMIP, consistent with the influence of evolving sea-surface temperature and sea ice. With only one member per configuration, part of the local pressure and wind pattern may still reflect internal variability. These maps therefore provide a baseline for ensemble testing under SSP2-4.5 rather than deterministic regional predictions.